electronics

MDPI

Article

Switchable Reflective Excitation Method for Rapid Characterization of Monopulse Comparators

Shu-Yu Lin [1,2], Ming-Hsiang Cho [2,*] and Jwo-Shiun Sun [1]

[1] Department of Electronic Engineering, National Taipei University of Technology, Taipei 106, Taiwan; sylin03@gmail.com (S.-Y.L.); jssun@ntut.edu.tw (J.-S.S.)
[2] Electronic Systems Research Division, National Chung-Shan Institute of Science and Technology, Taoyuan 325, Taiwan
* Correspondence: chominghsiang@gmail.com

Abstract

In high-precision tracking radars, the angular resolution depends critically on the amplitude and phase balance of the monopulse comparator. However, accurately and efficiently characterizing this highly integrated microwave component remains challenging, as its complex structure and high port count increase the difficulty of microwave testing. To achieve rapid measurement without compromising accuracy, this paper presents a novel characterization technique utilizing switchable reflective excitation signals. By employing the inherent reflected signals as internal excitation sources, this physical innovation allows for the simultaneous multiport input of a four-horn comparator. In addition, a switchable calibration window and a multiport matched load were designed to precisely control the boundary conditions directly at the reference plane of the device under test (DUT). Experimental validation on an X-band waveguide monopulse comparator demonstrates that the proposed methodology can promptly extract the intrinsic device characteristics. Good agreement between the theoretical predictions and measurement results confirms that the proposed technique provides a rapid and robust diagnostic solution for microwave measurement of monopulse comparators.

Keywords: calibration kits; magic tee; microwave measurement; monopulse antenna; monopulse comparator; reflective excitation; tracking radar; waveguide

1. Introduction

High-precision tracking radars rely heavily on the accuracy of their microwave feeding networks of antenna systems to acquire exact angular information of moving targets. As extensively documented in [1–6], monopulse radar architectures remain the gold standard for tracking applications, offering immunity to target amplitude fluctuations by extracting complete angular error information from a single pulse. At the core of these feeding networks is the monopulse comparator, which processes the received signals to generate the sum (Σ) and difference (Δ) channels. The electromagnetic integrity of this integrated microwave component is critical. Any amplitude or phase imbalance within the comparator directly diminishes the depth of the null in the antenna's difference pattern, thereby limiting the radar's angle error slope and overall tracking resolution.

To ensure that the performance of the comparator meets the system requirements, the precise microwave characterization of the fabricated components is essential. However, accurately and efficiently evaluating these multiport microwave networks presents

Check for updates

Received: 11 April 2026
Revised: 14 May 2026
Accepted: 16 May 2026
Published: 19 May 2026

Copyright: © 2026 by the authors. Licensee MDPI, Basel, Switzerland. This article is an open access article distributed under the terms and conditions of the Creative Commons Attribution (CC BY) license.

significant measurement challenges. Conventional characterization setups using a standard two-port vector network analyzer (VNA) are inefficient for such components. The complex structure and high port count of a four-horn monopulse comparator require repetitive mechanical reconnections, sequential port switching, and multiple short and match terminations to evaluate all signal reflection and transmission paths. This conventional port-by-port network analysis not only significantly increases the testing time but also introduces measurement inconsistencies at the waveguide interfaces, making rapid and reliable evaluation exceedingly difficult.

While multiport VNA extensions offer a viable alternative [7,8], monopulse comparator measurements often require seven or more ports, for which the necessary instrumentation is less commonly available. Moreover, the close proximity of the four feed horn apertures makes it mechanically unfeasible to simultaneously connect four bulky, rigid waveguide adaptors or transitions. Furthermore, the utilization of multiport measurements cables may introduce dynamic phase drifts and calibration complexities, which can critically degrade the measurement accuracy.

To overcome the aforementioned limitations and achieve rapid measurement without compromising accuracy, this paper proposes a novel characterization technique utilizing switchable reflective excitation signals. Instead of sequentially measuring individual ports, the proposed methodology integrates a custom-designed switchable reflective window and a multiport matched load to precisely control the boundary conditions directly at the reference plane of the DUT. By actively toggling these switchable states, the inherent reflected signals are efficiently repurposed as internal excitation sources. This physical innovation allows for the simultaneous multiport input of the four-horn comparator, effectively simulating its actual operation and dramatically reducing the measurement complexity.

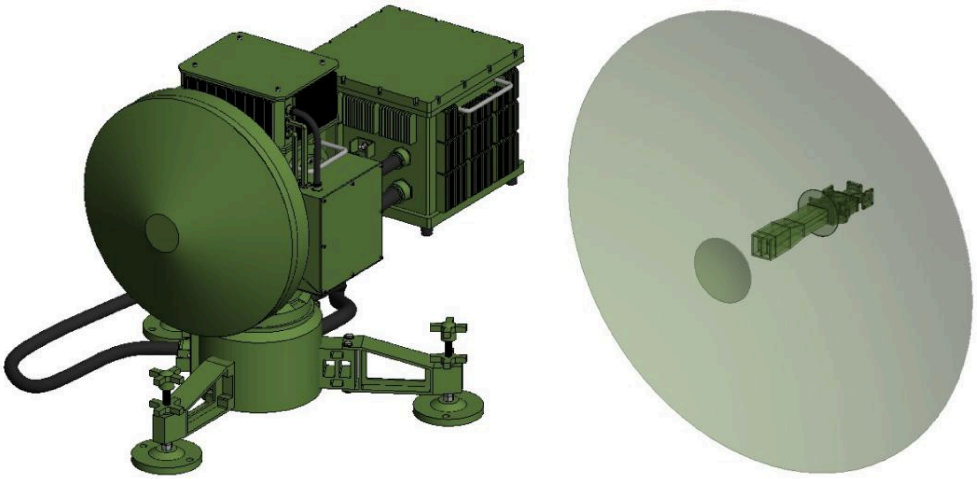
By directly extracting the intrinsic sum and difference characteristics under simultaneous excitation, and comparing these physical results with theoretical values, the highly-integrated comparator is rapidly evaluated. The remainder of this paper is organized as follows: Section 2 demonstrates the monopulse comparator architecture and details the proposed reflective excitation feeding method along with the custom-designed switchable calibration kits. Section 3 presents the experimental results and the quantitative comparison between the measured and theoretical values. Finally, Section 4 concludes this paper.

2. Switchable Measurement Technique for Microwave Characterization of Monopulse Comparator

This section details the theoretical foundation and the physical implementation of the proposed switchable characterization method. First, the system architecture and operational logic of the monopulse radar are introduced. Subsequently, the novel reflective excitation feeding method, which utilizes reflected signals to achieve simultaneous multiport excitation, is proposed for the first time. Finally, the custom-designed test fixtures are presented to demonstrate the practical realization of the proposed measurement framework.

2.1. Monopulse Antenna System

The performance of a precision tracking radar is fundamentally determined by its ability to resolve a target's coordinates. In this study, we use a mobile monopulse tracking radar system as an example to illustrate the proposed method. The computer-aided design (CAD) model of the tracking radar is depicted in Figure 1. The core of its tracking capability lies within the antenna assembly. Figure 1 provides a perspective view of a Cassegrain antenna [9] and its critical component—the monopulse comparator. As established in the literature, the physical symmetry of the comparator is the primary factor influencing the formation of the required beam patterns.



(**a**) (**b**)

Figure 1. CAD model of a mobile monopulse tracking radar. (**a**) External view of the tracking radar. (**b**) Perspective view of the Cassegrain antenna and monopulse comparator.

To further analyze the signal processing flow, a simplified architecture of the dual-channel monopulse radar system is presented in Figure 2.

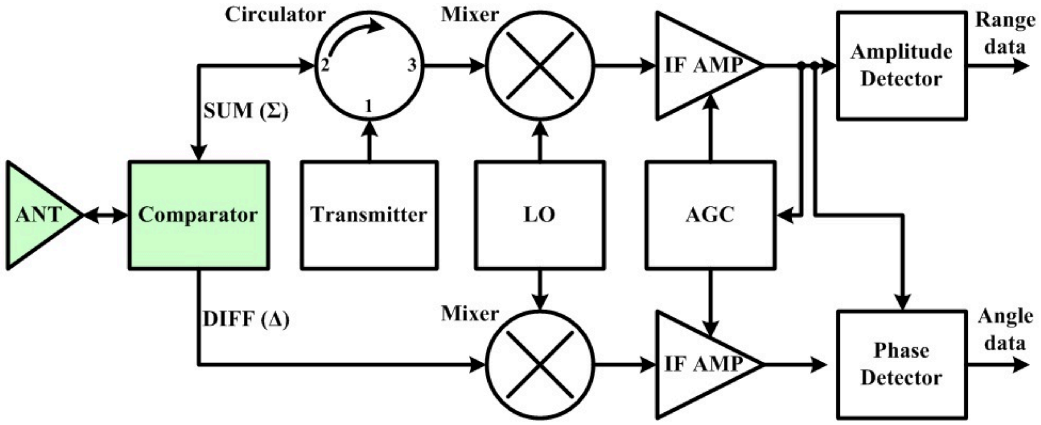


Figure 2. Block diagram of a dual-channel monopulse radar system.

In a typical amplitude-comparison monopulse tracking radar system, the antenna feed is divided into four symmetrical quadrants, denoted as A, B, C, and D. The monopulse comparator is a passive microwave network that synthesizes the signals received from these four quadrants to generate one sum channel (Σ) and two difference channels, which are azimuth difference (Δ_{AZ}) and elevation difference (Δ_{EL}), respectively. The fundamental arithmetic logic of the comparator can be expressed as:

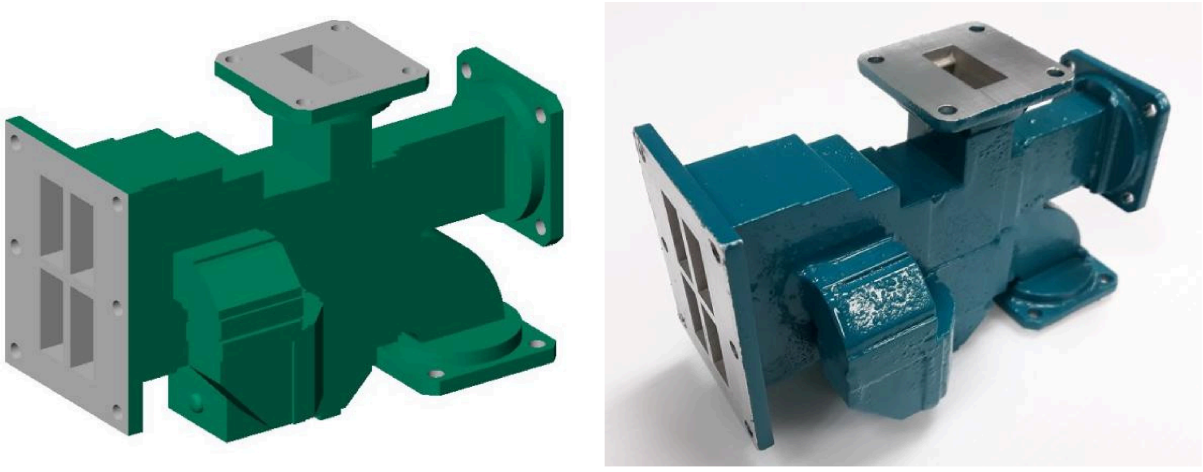
$$\Sigma = A + B + C + D, \tag{1}$$

$$\Delta_{AZ} = (A + D) - (B + C), \tag{2}$$

$$\Delta_{EL} = (A + B) - (C + D). \tag{3}$$

To achieve accurate characterization of this logic, the specific comparator network must be closely examined. The DUT in this study is a classic four-horn monopulse comparator. Figure 3 illustrates the external view of a comparator that comprises a highly integrated network of four waveguide magic-tee hybrids [10–12]. As detailed in Figure 4,

this interconnected topology creates complex internal signal paths, highlighting the need for advanced testing methodologies beyond conventional port-by-port measurements.



(**a**) (**b**)

Figure 3. Four-horn monopulse comparator. (**a**) CAD model. (**b**) Photograph.

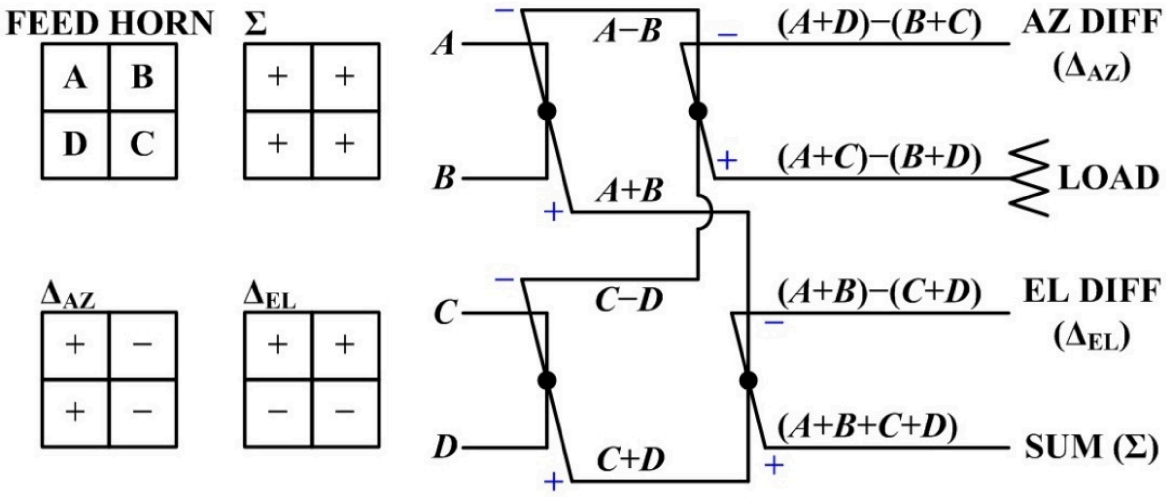
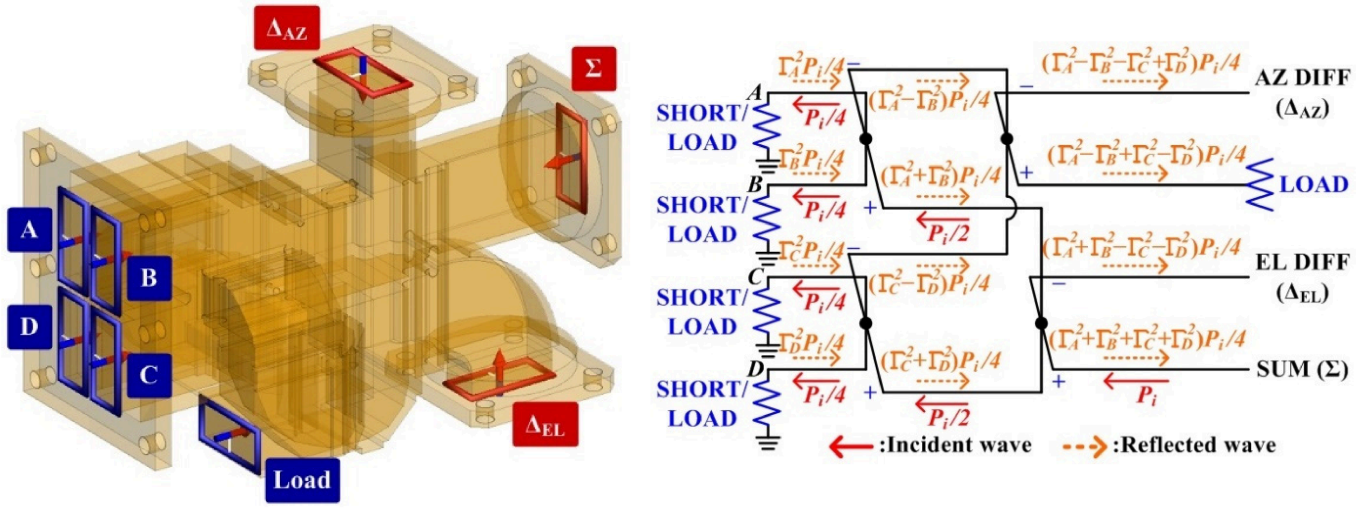


Figure 4. Schematic diagram of the four-horn monopulse comparator using waveguide magic-tee hybrids. The factors of $1/2^{0.5}$ and $1/2$ are omitted for simplicity.

2.2. Reflective Excitation Feeding Technique

To rapidly characterize the comparator, a novel reflective excitation feeding method is proposed, as illustrated in Figure 5. Figure 5a shows the specialized settings for the input/output ports and terminations established at the waveguide interfaces. The corresponding schematic diagram and signal flow analysis are depicted in Figure 5b. By systematically manipulating these reflective states, the setup introduces known boundary conditions, forcing the inherent signals to be reflected or absorbed and act as simultaneous internal excitation sources.

As shown in Figure 5b, the excitation power of incident wave P_i is equally distributed among ports A, B, C, and D through the magic-tee structures of the comparator. By utilizing the equally-divided power $P_i/4$ in conjunction with short circuits and matched loads, simultaneous multiport excitation is realized. Here, Γ_A, Γ_B, Γ_C, and Γ_D represent the reflection coefficients of ports A, B, C, and D, respectively.



(**a**) (**b**)

Figure 5. Proposed reflective excitation concept for microwave characterization of comparators. (**a**) Settings for input/output ports and terminations. (**b**) Schematic diagram and signal flow analysis.

The reflected signal power received at sum, azimuth difference, and elevation difference ports of monopulse comparator with switchable inputs are respectively denoted as $P_{r,\Sigma}$, $P_{r,\Delta AZ}$, and $P_{r,\Delta EL}$ and can be expressed as:

$$P_{r,\Sigma} = (\Gamma_A{}^2 + \Gamma_B{}^2 + \Gamma_C{}^2 + \Gamma_D{}^2)P_i/4, \quad (4)$$

$$P_{r,\Delta AZ} = (\Gamma_A{}^2 - \Gamma_B{}^2 - \Gamma_C{}^2 + \Gamma_D{}^2)P_i/4, \quad (5)$$

$$P_{r,\Delta EL} = (\Gamma_A{}^2 + \Gamma_B{}^2 - \Gamma_C{}^2 - \Gamma_D{}^2)P_i/4. \quad (6)$$

Based on the above signal flow analysis shown in Figure 5, the theoretical values of 13 calibration points for a four-horn monopulse comparator can be derived. As summarized in Table 1, the 13 possible excitation states represent the theoretical known boundaries (e.g., ideal shorts or matched loads) generated by the switchable fixtures [13–17]. Taking the single-input case as an example, assume that Port *A* is short-circuited while the sum port is excited, $P_{r,\Sigma}$, $P_{r,\Delta AZ}$, and $P_{r,\Delta EL}$ each have a value of $P_i/4$. Therefore, the values of Σ and Δ_{AZ}, and Δ_{EL} in the second row of Table 1 are all 1/4. Compared to prior work, we employ the reflected wave as simultaneous multiport excitation to derive the theoretical sum and difference values of a monopulse comparator. In addition, we normalize the maximum signal levels to 0 dB to align with the *S*-parameter measurements from the vector network analyzer.

2.3. Switchable Calibration Window and Multiport Matched Load

To physically implement the 13-state reflective excitation outlined in Table 1, custom-designed calibration kits were engineered. Standard waveguide test setups require repetitive mechanical connections, which inevitably introduce measurement inconsistencies. To resolve this, the proposed method employs a switchable reflective window and a multiport matched load. Figure 6 provides an exploded view of these components, illustrating the precise mechanical alignment and switchable termination states.

Table 1. Theoretical values of 13 calibration points for a four-horn monopulse comparator. Here the symbols ○ and × represent the input ports switched to short and matched load, respectively.

Switch Input	A	B	C	D	Σ		Δ_{AZ}		Δ_{EL}	
					Amp.	dB	Amp.	dB	Amp.	dB
A	○	×	×	×	1/4	−12.04	1/4	−12.04	1/4	−12.04
B	×	○	×	×	1/4	−12.04	−1/4	−12.04	1/4	−12.04
C	×	×	○	×	1/4	−12.04	−1/4	−12.04	−1/4	−12.04
D	×	×	×	○	1/4	−12.04	1/4	−12.04	−1/4	−12.04
AB	○	○	×	×	1/2	−6.02	0	−∞	1/2	−6.02
BC	×	○	○	×	1/2	−6.02	−1/2	−6.02	0	−∞
CD	×	×	○	○	1/2	−6.02	0	−∞	−1/2	−6.02
AD	○	×	×	○	1/2	−6.02	1/2	−6.02	0	−∞
ABC	○	○	○	×	3/4	−2.5	−1/4	−12.04	1/4	−12.04
BCD	×	○	○	○	3/4	−2.5	−1/4	−12.04	−1/4	−12.04
ACD	○	×	○	○	3/4	−2.5	1/4	−12.04	−1/4	−12.04
ABD	○	○	×	○	3/4	−2.5	1/4	−12.04	1/4	−12.04
ABCD	○	○	○	○	1	0	0	−∞	0	−∞

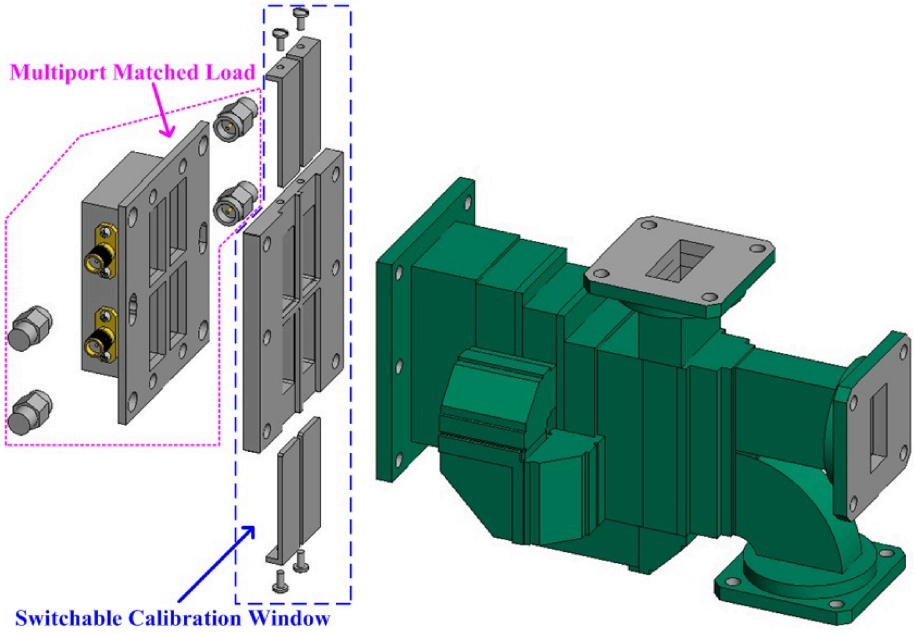
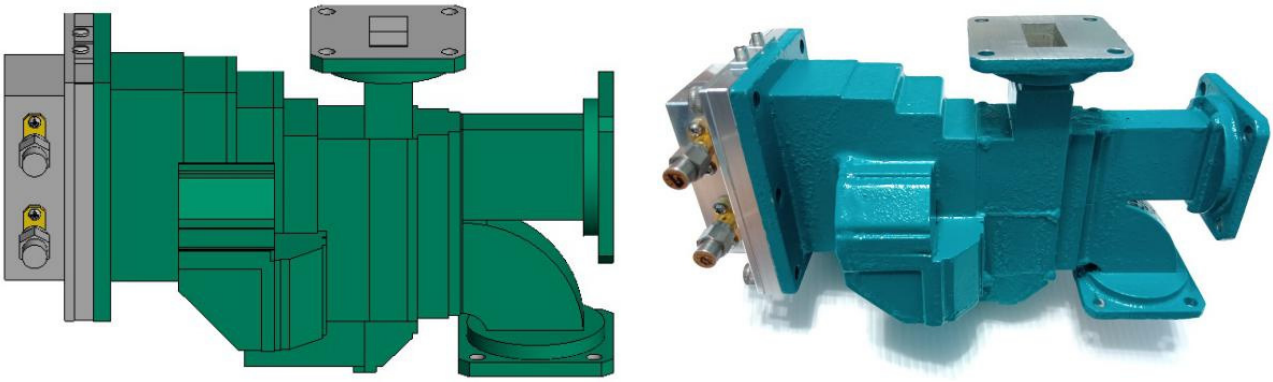


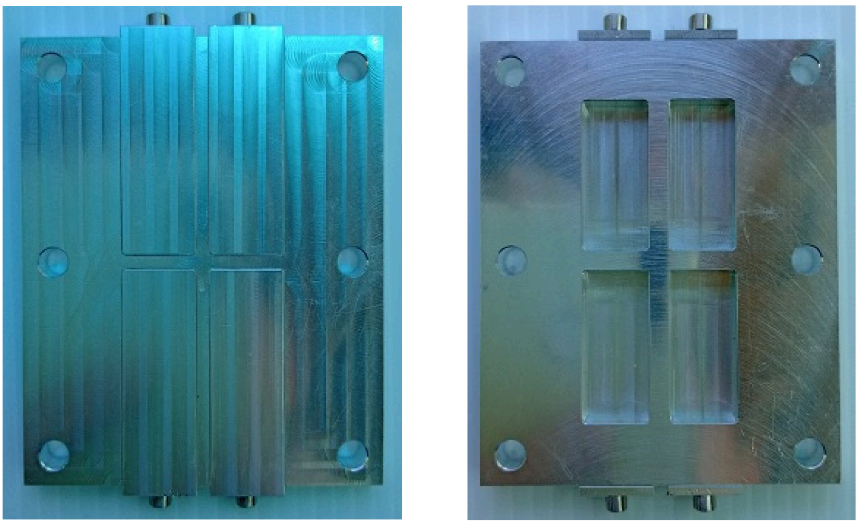
Figure 6. Exploded view of switchable calibration window and multiport matched load for rapid measurement of monopulse comparators.

The measurement configuration is presented in Figure 7, showing the CAD assembly model and the actual assembled setup. The core element enabling dynamic boundary modulation is the switchable reflective window, with its front and rear views detailed in Figure 8. This component allows rapid toggling of reflective signals directly at the reference plane without physically disconnecting the DUT and waveguide adaptors. Furthermore, to provide the reference impedance, a specialized multiport matched load is utilized, as shown in Figure 9. Together, these highly integrated fixtures facilitate the rapid acquisition of the signal states, enabling simultaneous multiport excitation while fundamentally eliminating non-repeatable mechanical and measurement errors.



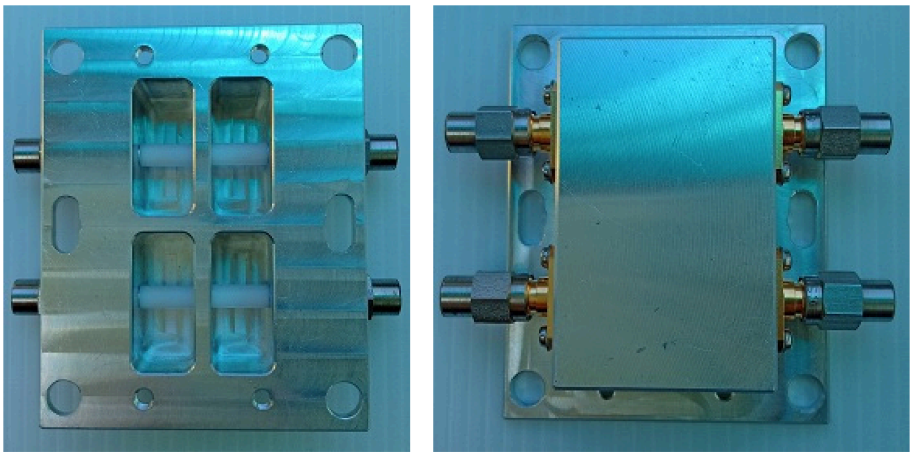
(**a**) (**b**)

Figure 7. Assembled views of switchable calibration window and multiport matched load for rapid measurement of monopulse comparators. (**a**) CAD model. (**b**) Photograph.



(**a**) (**b**)

Figure 8. Photograph of switchable calibration window. (**a**) Front view. (**b**) Rear view.



(**a**) (**b**)

Figure 9. Photograph of multiport matched load. (**a**) Front view. (**b**) Rear view.

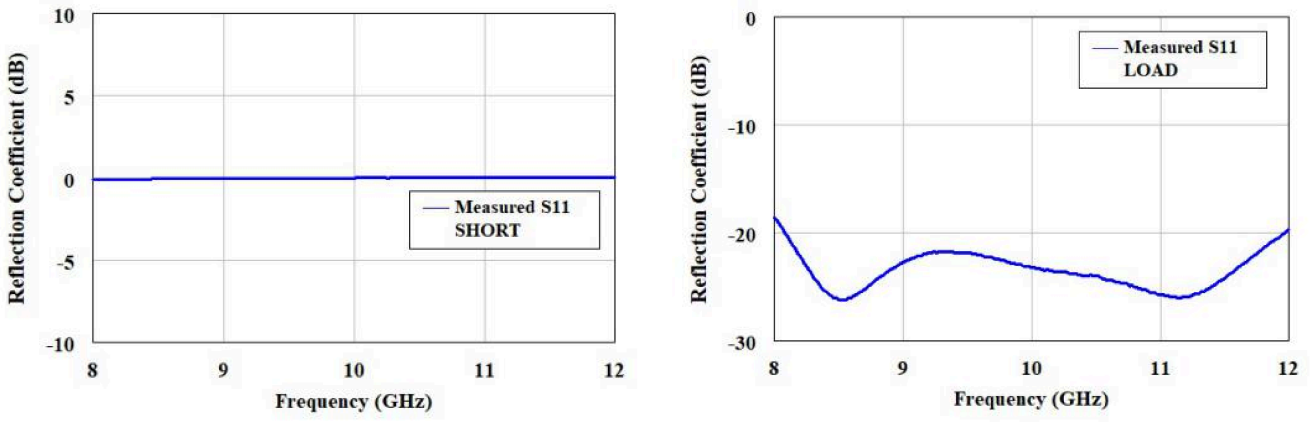
3. Results and Discussion

This section presents the experimental validation of the proposed characterization method. By utilizing the inherent reflected signals as internal excitation sources, the mi-

crowave characteristics of the X-band waveguide monopulse comparator can be accurately extracted. To evaluate the hardware performance and validate the simultaneous excitation concept, the extracted measurement data are systematically compared with the theoretical results.

3.1. Experimental Results of Switchable Calibration Kits

Before characterizing the comparator, the fundamental microwave responses of the custom-designed switchable fixtures designed for X-band applications should verified, as they provide the critical boundaries for generating the required reflected signals. Figure 10 presents the measured reflection coefficients of the switchable reflective window and the multiport matched load. The closed switchable window must provide a highly stable reflection boundary across the operational bandwidth, while the multiport matched load must exhibit good return loss to ensure the absorption boundary condition. The robust performance of these fixtures guarantees that the distinct reflective excitation states are accurately established for the subsequent microwave measurements.



(**a**) (**b**)

Figure 10. Measured reflection coefficients of switchable calibration kits. (**a**) Switchable calibration window (closed). (**b**) Multiport matched load.

3.2. The 13-Point Calibration Results of the Waveguide Monopulse Comparator

Below are the measurement results for the four-horn monopulse comparator designed at 10 GHz. Here we set Port 1, Port 2, and Port 3 as sum, azimuth difference, and elevation difference, respectively. The extracted sum signal (Σ) of the comparator, illustrated in Figure 11, demonstrates optimal in-phase power combining. The signal intensity progressively and stably increases as the reflective excitation transitions from a single input to all four simultaneous inputs. The discrepancy between measured data and theoretical values increases as the operating frequency deviates from the center frequency (10 GHz).

Furthermore, the azimuth and elevation difference channels (Δ_{AZ} and Δ_{EL}), plotted in Figures 12 and 13, respectively, rely strictly on the out-of-phase cancellation of the simultaneous excitation signals. As observed in the multi-input excitation states, the comparison between the theoretical and measured difference signals demonstrates a high degree of agreement, especially near the center frequency.

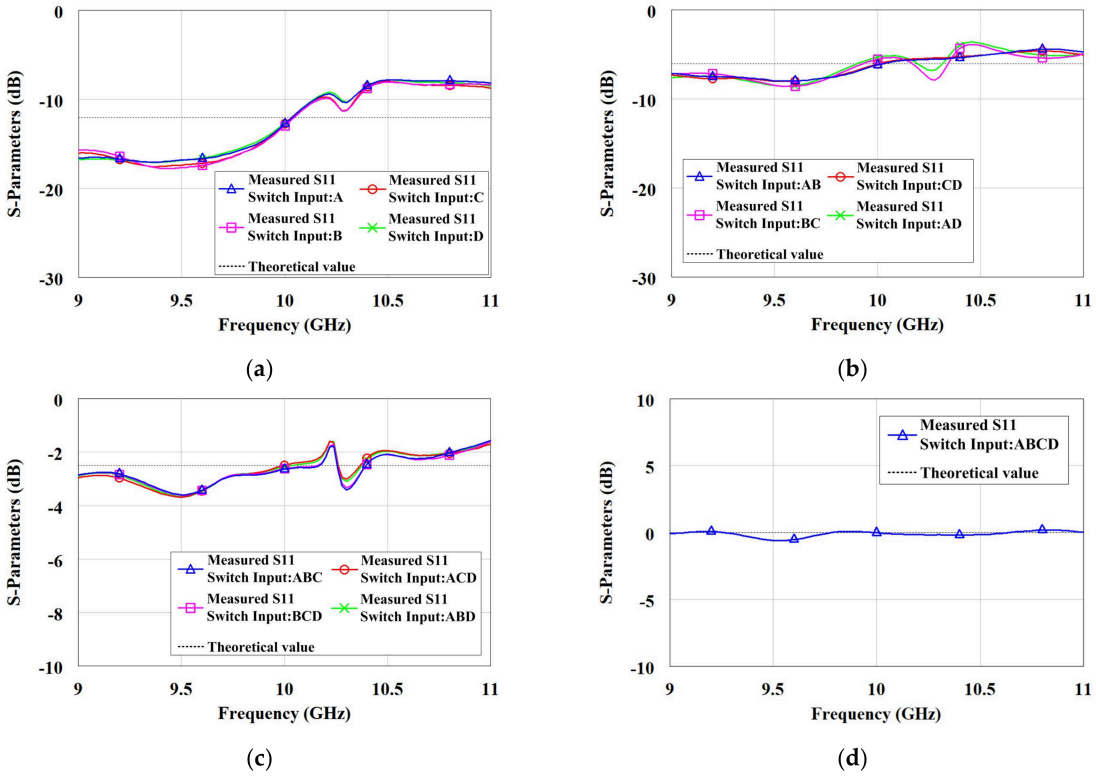


Figure 11. Measured sum signal of monopulse comparator with switchable inputs. (**a**) Single input. (**b**) Two inputs. (**c**) Three inputs. (**d**) Four inputs. Port 1: Σ, Port 2: Δ_{AZ}, Port 3: Δ_{EL}.

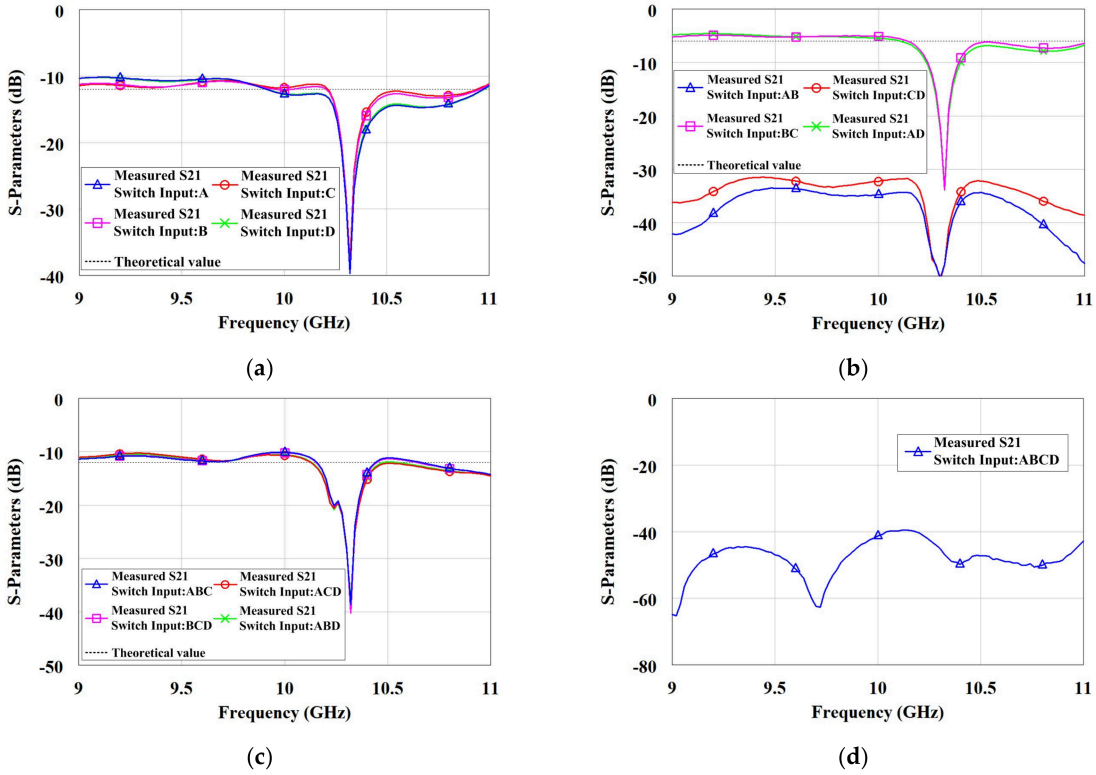


Figure 12. Measured azimuth difference signal of monopulse comparator with switchable inputs. (**a**) Single input. (**b**) Two inputs. (**c**) Three inputs. (**d**) Four inputs. Port 1: Σ, Port 2: Δ_{AZ}, Port 3: Δ_{EL}.

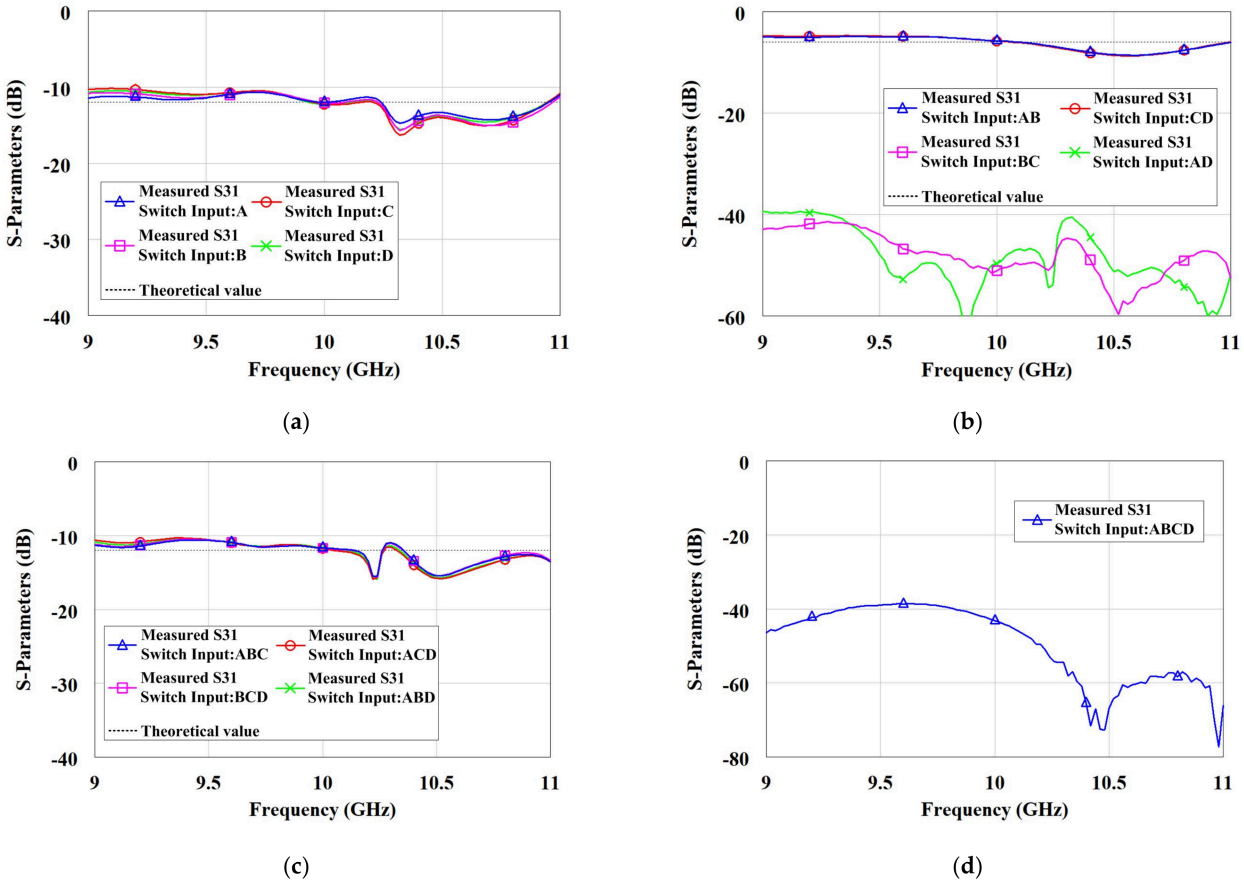


Figure 13. Measured elevation difference signal of monopulse comparator with switchable inputs. (**a**) Single input. (**b**) Two inputs. (**c**) Three inputs. (**d**) Four inputs. Port 1: Σ, Port 2: Δ_{AZ}, Port 3: Δ_{EL}.

To provide a precise quantitative evaluation, the extracted sum and difference data at the radar's center frequency of 10 GHz are summarized in Table 2. As we can see, the errors between the measured results and theoretical values for the single-input cases are all within 1 dB. The discrepancies are within acceptable limits. They are primarily attributed to structural design and assembly misalignment, which are typical in this frequency range. The low values observed in the difference channels, ranging from −32.31 dB to −51.01 dB, represent the null depth of the monopulse comparator. These values are well above the system's noise floor (approximately −80 dBm in our setup) and fall within the dynamic range of the network analyzer, ensuring measurement reliability. Such deep nulls imply that the comparator possesses good amplitude and phase balance between its internal paths. It indicates that the signals from the antenna ports are effectively canceled at the difference ports due to the high structural symmetry of the magic-tee network. The measured sum signal level of the four-input case is very close to 0 dB, demonstrating the comparator's superior performance of power distribution and combination This close correlation between the theoretical model and the physical implementation firmly validates the effectiveness of the proposed switchable characterization method.

As shown in Figure 12, a significant transmission null of −30 to −50 dB is consistently observed near 10.3 GHz, regardless of the input state. To further investigate this phenomenon, high-frequency electromagnetic field analysis was performed on the component. For simplicity, without loss of generality, we consider the case with a single input port. As shown in the simulation results in Figure 14, a significant transmission null near 10.5 GHz indeed occurs in the azimuth difference data, which is in good agreement with the measured data. As shown in the electric-field distribution of the monopulse comparator

in Figure 15, almost no energy passes through the upper azimuth port when resonance occurs. This is due to the structural differences between the magic tees used for the azimuth and elevation ports; consequently, the elevation port data does not exhibit resonance issues. According to the data in Figures 11 and 14, we also observed that the sum signal under single-input conditions exhibits significant frequency-dependent fluctuations. To achieve an extremely compact monopulse comparator design, constraints on the structure and integration of multiple magic tees are inevitable, which consequently restricts the operating bandwidth of the component.

Table 2. Measured and theoretical sum and difference data of a comparator designed at 10 GHz.

Switch Input	Σ (dB) Measured at 10 GHz	Σ (dB) Theoretical Value	Δ_{AZ} (dB) Measured at 10 GHz	Δ_{AZ} (dB) Theoretical Value	Δ_{EL} (dB) Measured at 10 GHz	Δ_{EL} (dB) Theoretical Value
A	−12.72	−12.04	−12.70	−12.04	−12.00	−12.04
B	−12.97	−12.04	−12.00	−12.04	−12.06	−12.04
C	−12.73	−12.04	−11.72	−12.04	−12.25	−12.04
D	−12.65	−12.04	−12.63	−12.04	−12.29	−12.04
AB	−6.17	−6.02	−34.74	−∞	−5.73	−6.02
BC	−5.52	−6.02	−5.11	−6.02	−51.01	−∞
CD	−6.07	−6.02	−32.31	−∞	−5.80	−6.02
AD	−5.32	−6.02	−5.46	−6.02	−49.65	−∞
ABC	−2.64	−2.5	−10.14	−12.04	−11.65	−12.04
BCD	−2.61	−2.5	−10.22	−12.04	−11.67	−12.04
ACD	−2.49	−2.5	−10.71	−12.04	−11.75	−12.04
ABD	−2.54	−2.5	−10.60	−12.04	−11.66	−12.04
ABCD	0.004	0	−41.27	−∞	−43.18	−∞

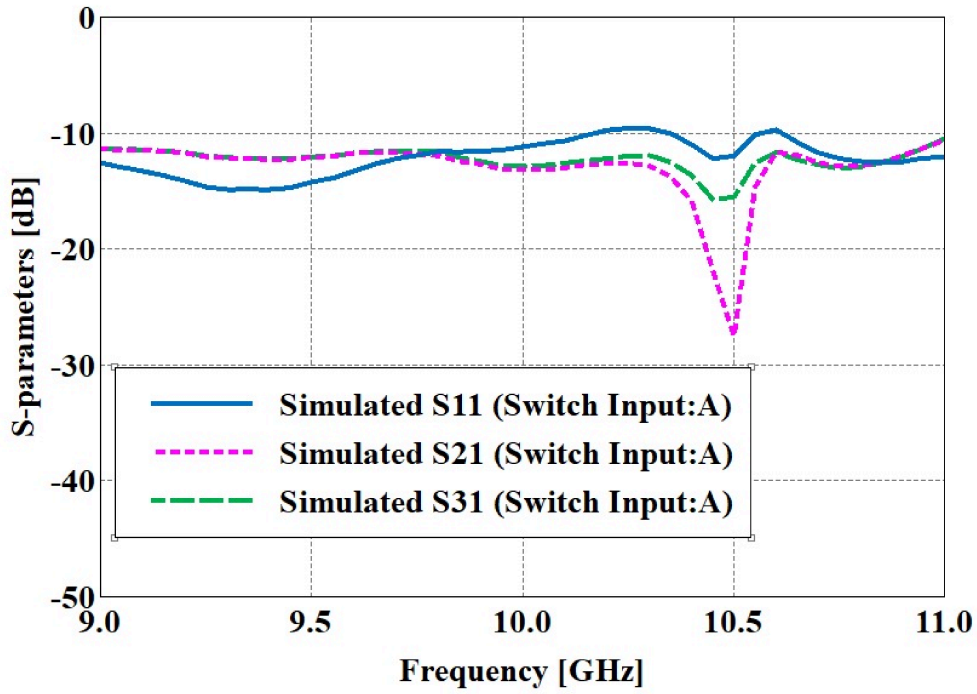
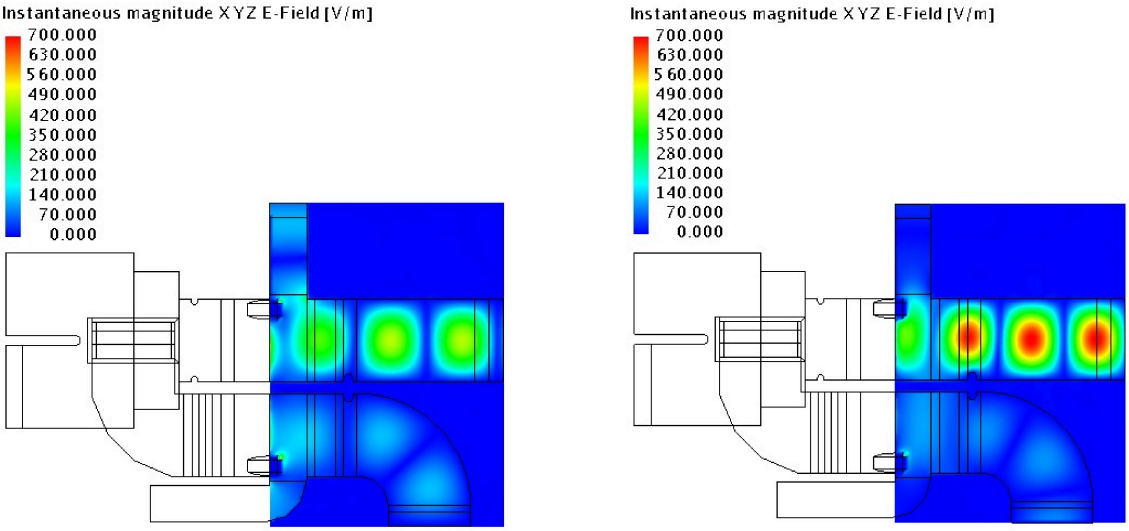


Figure 14. Simulated sum (S11), azimuth difference (S21), and elevation difference (S31) data of monopulse comparator with single input (Port A is short-circuited while the sum port is excited).



(**a**) (**b**)

Figure 15. Electric-field distribution of the four-horn monopulse comparator with single input (Port A is short-circuited while the sum port is excited) simulated at (**a**) designed frequency (10 GHz) and (**b**) resonant frequency (10.5 GHz).

4. Conclusions

This paper has presented a novel reflective excitation technique specifically designed to overcome the measurement inefficiencies and physical challenges associated with highly integrated, high-port-count monopulse comparators. By developing a custom switchable reflective window and a multiport matched load, the proposed methodology transforms inherent reflected signals into internal excitation sources. This physical hardware innovation successfully enables the simultaneous multiport excitation of the device under test, fundamentally eliminating the need for tedious, sequential port-by-port microwave measurements and the associated mechanical and measurement errors.

Experimental characterization of an X-band four-horn comparator rigorously validated the efficacy of this approach. The intrinsic sum and difference channel responses were rapidly extracted under true operational boundary conditions. Quantitative analysis, particularly at the 10 GHz center frequency, demonstrated close agreement between the measurement data and the theoretical predictions. Ultimately, this simultaneous multiport excitation framework provides a rapid, accurate, and robust diagnostic solution for evaluating complex monopulse comparator and ensuring the high angular resolution demanded by tracking radar systems.

Author Contributions: Conceptualization, M.-H.C., S.-Y.L. and J.-S.S.; methodology, M.-H.C. and S.-Y.L.; software, S.-Y.L. and M.-H.C.; validation, S.-Y.L. and M.-H.C.; formal analysis, M.-H.C. and S.-Y.L.; investigation, M.-H.C. and S.-Y.L.; resources, M.-H.C. and S.-Y.L.; data curation, S.-Y.L. and M.-H.C.; writing—original draft preparation, S.-Y.L. and M.-H.C.; writing—review and editing, M.-H.C. and S.-Y.L.; visualization, M.-H.C. and S.-Y.L.; supervision, M.-H.C. and J.-S.S.; project administration, M.-H.C. and S.-Y.L.; funding acquisition, S.-Y.L. and J.-S.S. All authors have read and agreed to the published version of the manuscript.

Funding: This research received no external funding.

Data Availability Statement: All data are included within manuscript.

Conflicts of Interest: The authors declare no conflicts of interest.

Abbreviations

The following abbreviations are used in this manuscript:

DUT	Device under test
VNA	Vector network analyzer
CAD	Computer-aided design

References

1. Skolnik, M.I. *Radar Handbook*, 3rd ed.; McGraw-Hill: New York, NY, USA, 2008; pp. 9.1–9.6.
2. Sherman, S.M.; Barton, D.K. *Monopulse Principles and Techniques*, 2nd ed.; Artech House: Norwood, MA, USA, 2011; pp. 2–16.
3. Huang, G.-L.; Zhou, S.-G.; Chio, T.-H.; Yeo, T.-S. Two types of waveguide comparator for wideband monopulse antenna array application. In *2015 IEEE 5th Asia-Pacific Conference on Synthetic Aperture Radar (APSAR), Singapore, 1–4 September 2015*; IEEE: New York, NY, USA, 2015; pp. 264–266. [CrossRef]
4. Liu, B.; Hong, W.; Kuai, Z.; Yin, X.; Luo, G.; Chen, J.; Tang, H.; Wu, K. Substrate integrated waveguide (SIW) monopulse slot antenna array. *IEEE Trans. Antennas Propag.* **2009**, *57*, 275–279. [CrossRef]
5. Singh, A.K. A low cost, low side lobe and high efficiency non-orthogonally coupled slotted waveguide array antenna for monopulse radar tracking. In *IEEE Antennas Propagation Society International Symposium*; IEEE: New York, NY, USA, 2005; pp. 732–735. [CrossRef]
6. Zink, M.; Ottl, H.; Freeman, A. Design of a monopulse SAR system for the determination of elevation angles. *IEEE Trans. Geosci. Remote Sens.* **1994**, *32*, 1198–1201. [CrossRef]
7. Ferrero, A.; Teppati, V.; Garelli, M.; Neri, A. A Novel Calibration Algorithm for a Special Class of Multiport Vector Network Analyzers. *IEEE Trans. Microw. Theory Tech.* **2008**, *56*, 693–699. [CrossRef]
8. Ruttan, T.G.; Grossman, B.; Ferrero, A.; Teppati, V.; Martens, J. Multiport VNA measurement. *IEEE Microw. Mag.* **2008**, *9*, 56–69. [CrossRef]
9. Stutzman, W.L.; Thiele, G.A. *Antenna Theory and Design*, 2nd ed.; John Wiley & Sons: Hoboken, NJ, USA, 1998; pp. 335–338.
10. Pozar, D.M. *Microwave Engineering*, 3rd ed.; John Wiley & Sons: Hoboken, NJ, USA, 2005; p. 361.
11. Wu, J.; Wang, C.; Guo, Y. Ridged Waveguide Magic Tees Based on 3-D Printing Technology. *IEEE Trans. Microw. Theory Tech.* **2020**, *68*, 4267–4275. [CrossRef]
12. Ren, L.; Shu, Y. Full-Band Millimeter Wave Waveguide Magic Tees and Power Dividers for Manufacturing Ability. In Proceedings of the IEEE 2021 51st European Microwave Conference (EuMC), London, UK, 4–6 April 2022; pp. 229–232. [CrossRef]
13. Harbater, Z.; Margalit, A. A Bit System that Guarantees Better Accuracy for Monopulse Antenna Detection Systems. *IEEE Antennas Propag. Mag.* **2000**, *42*, 82–86. [CrossRef] [PubMed]
14. Freeman, A.; Zink, M. An Application of the Monopnlse principle to determining elevation angles in SAR images. *IEEE Trans. Geosci. Remote Sens.* **1994**, *32*, 616–625. [CrossRef]
15. Lin, F.-L.C.; Kretschmer, F.F. Angle measurement in the presence of mainbeam interference. *IEEE Aerosp. Electron. Syst. Mag.* **1990**, *5*, 19–25. [CrossRef]
16. Xue, H.; Kezys, V.; Litva, J. Smart antenna calibration for beamforming. *IEEE Antennas Propag. Soc. Int. Symp.* **1998**, *3*, 1458–1461. [CrossRef]
17. Akhoondmahdi, Z.; Bakhtafrouz, A. Design and Implementation of Wideband Monopulse Comparator Based on Inverted-Microstrip Gap Waveguide Technology. *IEEE Access* **2024**, *12*, 134926–134936. [CrossRef]

Disclaimer/Publisher's Note: The statements, opinions and data contained in all publications are solely those of the individual author(s) and contributor(s) and not of MDPI and/or the editor(s). MDPI and/or the editor(s) disclaim responsibility for any injury to people or property resulting from any ideas, methods, instructions or products referred to in the content.